

CALTECH STUDENT-FACULTY PROGRAMS

Final Report

Steven DOURMASHKIN

Mentor: Laura JONES

Program Coordinator: Linda RODGERS

Summer 2015

1. ABSTRACT

The development of the Small Satellite Dynamics Testbed (SSDT) is tied to a growing interest in small satellites as low-cost technology demonstrators for universities as well as viable platforms of traditional mission objectives for spacecraft developers. Unlike conventional spacecraft testbeds, the SSDT accommodates the reduced sizes and budgets of small satellites, using planar air bearings to provide frictionless motion for one rotational and two translational degrees of freedom as well as a spherical air bearing for all three rotational degrees of freedom, in turn simulating an in-orbit environment. In order for small satellite teams to correctly interpret results of the SSDT, however, friction as well as other disturbances that prevent the system from perfectly replicating a space-like environment must be characterized. This report describes the approach towards a test plan that lays out the complete set of tests that, once conducted, will provide enough data to develop an accurate model of the disturbance forces acting on the system. In addition, the report describes the mechanical design of the spherical air bearing mount and mass properties simulator, as well as the analysis performed for some of the first costumers of the SSDT.

2. BACKGROUND

This summer, I worked on the SmallSat Dynamics Testbed: a new testbed facility at the Jet Propulsion Laboratory that will be used to analyze the dynamics and controls of spacecraft under 30 kg by creating an environment similar to that in orbit. My primary task was to help Laura Jones characterize the friction within the system as well as other imperfections that prevent the testbed from perfectly replicating a space-like environment. The development of the SmallSat Dynamics Testbed is tied to the growing interest in small satellites, which are being used as low-cost technology demonstrators by universities as well as viable platforms for traditional mission objectives by spacecraft developers. These satellites typically follow the CubeSat standard: 1kg in a 10cm cube. Because traditional spacecraft testbeds are not designed for these low weights and sizes, there has been a push to develop new testbeds specifically designed for small satellites. In particular, because small satellites often have a relatively low budget, air bearing testbeds, which are less complicated, large, and expensive than, for instance, neutral buoyancy and robotically-controlled testbeds, have been commonly favored. Air bearing systems create a thin film of gas adjacent to a smooth, leveled surface to establish low-friction motion and, in turn, simulate a free-floating satellite in space in one rotational and two translational degrees of freedom.

During my internship, Dr. Jones and her lab members were still designing and assembling the sled that houses the planar air bearings (i.e., the planar carriage) onto which a satellite being tested will be mounted. Once this task is complete, they will run the tests and analysis scripts that I have designed to characterize the system. If my efforts are successful, future CubeSat and SmallSat projects will be able to correctly interpret the results of the SmallSat Dynamics Testbed since they will be able to accurately take into account friction and other disturbances in the system.

After finishing the test plan, I had worked on a number of side projects for the SSDT. These primarily include fixing errors and adding additional functionality to the Team X_c ACS GUI, as well as performing its verification and validation (V&V); developing the framework and first-order model of the inflatable antenna's expected dynamics when being tested on the planar carriage; implementing and beginning the V&V for a Jovian magnetic field model; designing a mass properties simulator and corresponding MATLAB GUI; and, most importantly, designing a spherical air bearing carriage capable of supporting up to a 6U CubeSat. These projects, as well as my approach towards the effective friction characterization test plan, are described throughout this report.

3. METHODS AND APPROACH

3.a. **Effective Friction Characterization Test Plan.** As confirmed by an engineer from OAV Air Bearings, the friction that acts on the air bearings is related to the shear stress in the thin film of air created by the outflowing gas molecules; since the bearings do not make physical contact with the surface, sliding friction (i.e., the coefficients of static and kinetic friction) are irrelevant for this system. Thus, the frictional force applied to the moving SSDT is related to the shear resulting from Couette flow,

$$(1) \quad F = \mu A \frac{u}{y},$$

where μ is the viscosity of the pressurized gas, A is the total contact area of the air bearings, u is the speed of the planar carriage, and y is the separation distance between the air bearings and the surface. In addition to friction, other disturbance forces arise primarily from the irregularities in the testing surface, including a steadily and/or locally uneven surface and groves in between the connections of the surface. The procedures described in my planar carriage test plan address all of these sources of disturbance force.

Using the equation above as a simplified model of the frictional disturbances, the first set of tests that I designed for my test plan consists of spinning the planar carriage up to two different constant velocities using a set of reaction wheels (the BCT 100 mN m/s) and waiting for the frictional forces opposing the planar carriages rotational motion to cause the planar carriage to come to rest. If the float time of the SSDT permits, the wheels will then be commanded off while the SSDT is still in use, in turn repeating the process in the opposite spin direction; otherwise, the test will be repeated by commanding the wheels to spin in the opposite direction. Throughout the test, the angular velocity of the planar carriage will be accurately and continuously recorded by the VICON system, which will allow the profile of friction as a function of velocity to be obtained; additional measurements will be obtained using an onboard IMU (the KVH 1750). This set of tests will be repeated by changing the separation distance, y , between the air bearings and the testing surface. This will be achieved by incrementally adding mass to the SSDT and repeating the first test described above, as well as altering the

input pressure to the air bearings. Since the planar carriage is designed to support at most 30 kg, the range of loads to be tested will be 0 kg (i.e., no load) to 30 kg (TBC) in order to test the extremes to, in turn, verify a relationship between mass and frictional force.

The second set of tests will involve manually pushing the planar carriage to an initial translational velocity, and using the VICON system as well as the onboard IMU to measure and observe any change of the carriages velocity throughout its trajectory. Two approximate initial velocities slow (5 cm/s) and fast (20 cm/s) using different carriage loads will be applied to observe the effects of velocity and mass (and, in turn, film layer thickness). The carriage will be pushed horizontally along the Formation Control Testbed (FCT), perpendicular to the groves of the testbeds tiles. To determine the effects of any irregularities in the FCT, the carriage will be pushed in both horizontal directions. Further, to test irregularities in the planar carriage that might cause disturbances, the carriage will be pushed in two different initial configurations: the first with one of the carriages edges facing forward, and the other with the same edge facing backwards.

To verify the success of a given test, enough velocity data points must be collected to observe a non-zero change in velocity with high confidence. This is quantified by rejecting the null hypothesis (i.e., a zero change in velocity) with $3\text{-}\sigma$ confidence. To do so, the equation of motion modeled by Equation 1 is solved and linearized, as follows:

$$\begin{aligned}
 F &= m\dot{u} = -\frac{\mu A}{y}u \\
 u &= Ce^{\frac{\mu A}{my}t} \\
 \log(u) &= \log(C) + \frac{\mu A}{my}t
 \end{aligned}
 \tag{2}$$

The null hypothesis can be rejected when

$$\Phi\left(\frac{\beta - \beta_0}{\sigma\sqrt{S_{xx}}}\right) > t_{\alpha/2, n-2},
 \tag{3}$$

where β is the sample linearized velocity slope, β_0 is the linearized velocity slope of the null hypothesis (i.e., zero), σ is the sample standard deviation of velocity data (determined by the precision of the VICON system), $t_{\alpha/2, n-2}$ is the t-value corresponding to a $3\text{-}\sigma$ confidence level, and S_{xx} is the sample variance found using:

$$S_{xx} = \sum_{i=1}^n (x - \bar{x})^2
 \tag{4}$$

All tests specified in the test plan will be performed in the Formation Control Testbed (FCT), located in building 199. I will be the test conductor, and will need a testing buddy; Pavel and/or Carl will be present to oversee the tests and provide support with the FCT; SSDT support will be present to send commands to the reaction wheels, receive data from the onboard IMU, and set up and run the VICON system; and, Kevin

will be on call. The reaction wheels and IMU of the XACT will be used. The first set of tests will take approximately one day to complete, while the second may take up to two days. A thorough list of tests following the approach stated above has been developed.

3.b. **Team X_c ACS GUI.** The ACS GUI Excel spreadsheet, used by JPL's Team X_c to analyze and validate their ACS designs, was the first task I had completed within this past month. I was responsible for formatting the spreadsheet to name each variable used in each equation, allowing the calculations to be more clearly understood. While working on this spreadsheet, I was able to discover and correct several errors in the calculations, as well as improve the spreadsheet's capabilities. Besides working on the Excel spreadsheet, I listed and cited each equation used in the spreadsheet, in addition to describing each of their variables. Working on the ACS GUI Excel spreadsheet has been an iterative process, for which I have sent revisions to Swati Mohan and Shawn Johnson who have been in turn sending back suggested changes and improvements.

3.c. **Inflatable Antenna Analysis.** Next, I had worked with Alessandra Babuscia on modeling the performance of her inflatable antenna on the SSDT planar carriage. This task involved developing a MATLAB program to calculate the motion of the antenna subjected to torque commanded to the reaction wheels on-board the carriage (specified by a .csv file containing torque values and the time at which they are applied) and aerodynamic drag, given the material properties and characteristics of the antenna. The aerodynamic drag along the antenna as a function of axial distance from its connection to the planar carriage was solved for using the drag equation,

$$(5) \quad F_{drag} = \frac{1}{2} \rho u^2 C_d A.$$

Given an infinitesimal segment of the antenna at an axial distance x of width dx , the differential drag on the antenna is solved as follows:

$$(6) \quad \begin{aligned} T_{drag} &= \int_0^h x dF_{drag} \\ &= \int_0^h x \frac{1}{2} \rho (\dot{\phi} x)^2 C_d \left(\frac{D}{h} dx \right) \end{aligned}$$

$$(7) \quad = \frac{1}{10} \rho C_d \dot{\phi}^2 D h^4$$

where $\dot{\phi}$ is the angular velocity of the antenna, and D and h are the diameter and height of the antenna modeled as a cone. By integrating the drag force along the antenna, the torque about the rotation point due to drag is found to be

$$(8) \quad T_{drag} = \frac{1}{10} \rho C_d \dot{\phi}^2 h^4.$$

The direction of this resultant torque is in the opposite direction of the antenna's rotation.

Shown below in Figure 1, the MATLAB graphical user interface (GUI) that was developed calculates the motion of the inflatable antenna using two different models: the Flexible Beam model, which represents the antenna as a flexible beam, and the Rigid Beam, Torsional Spring model, which represents the antenna as a rigid object subjected to a torsional spring force at its connection to the planar carriage. While the Flexible Beam model is still being implemented, the Rigid Beam, Torsional Spring model implements a torsional spring force on the antenna,

$$(9) \quad T_{spring} = k(\theta - \phi),$$

where k is a modeled torsional spring constant, and θ and ϕ are the angles of a reference direction on the planar carriage and antenna (which are initially aligned). After solving the equations of motion using MATLAB's `ode45`, the solution is animated, and the inputted carriage torques and the pointing errors calculated throughout the simulation are plotted towards the lower-right corner of the GUI. Using this GUI, we will be able to determine whether or not the planar carriage can supply enough torque required to move the inflatable antenna as desired by Alessandra, as well as understand the drag force acting on the antenna and, in turn, model its effects in the main SSDT simulator.

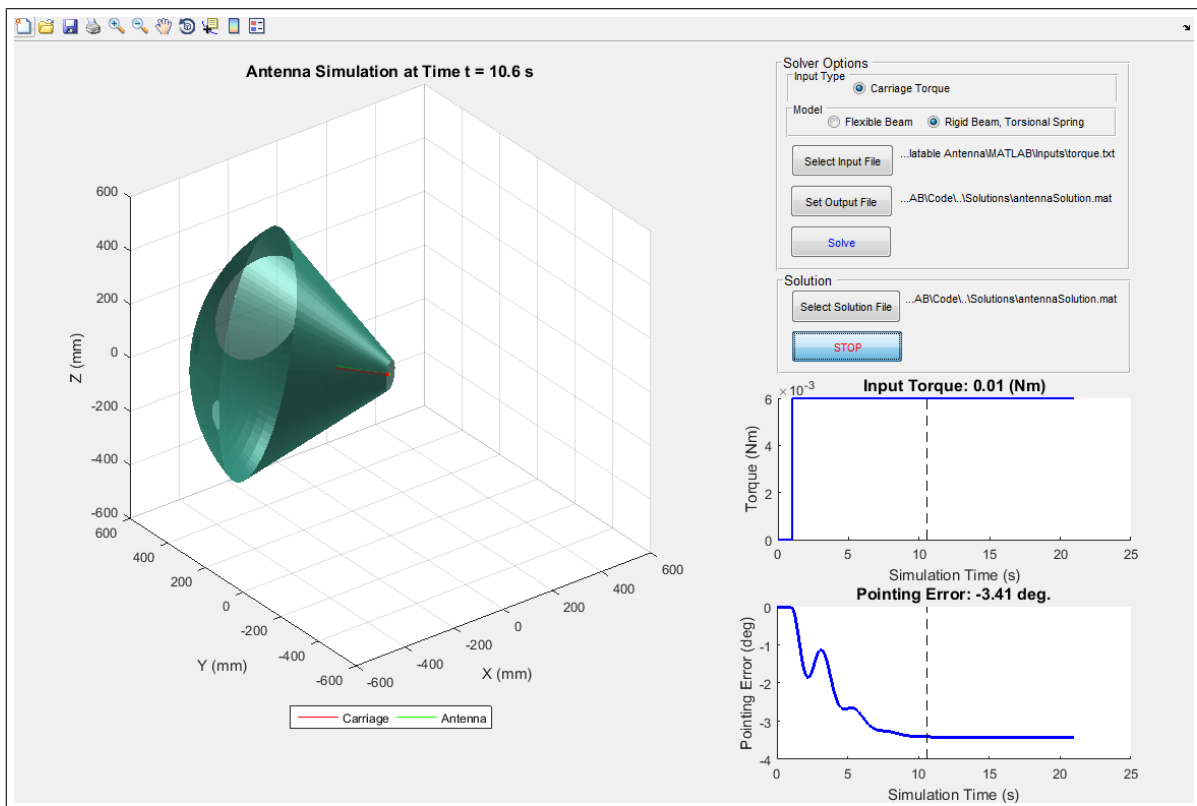


FIGURE 1. Antenna GUI developed for Alessandra Babuscia, a customer of the SSDT.

3.d. Jovian Magnetic Field Analysis. Another MATLAB GUI I have developed is used to illustrate Jupiter's magnetic field in order to verify the implementation of the VIP 4 mathematical model, which is applied to calculate the magnetic field in 3D space. As explained by Chapman and Bartels [2], the traditional spherical harmonic expansion of a scalar potential function V is given by

$$(10) \quad V = a \sum_{n=1}^{n_{max}} \left(\frac{a}{r}\right)^{n+1} \sum_{m=0}^n P_n^M \cos \theta (g_n^m \cos m\phi + h_n^m \sin m\phi),$$

where a is the equatorial radius of Jupiter, r is the radial distance from Jupiter's center, and θ and ϕ are the colatitude and longitude, respectively [3]. By taking the gradient of the scalar potential function, one can obtain the magnetic field:

$$(11) \quad \mathbf{B} = -\nabla V$$

Equation 11 is expanded as follows:

$$(12) \quad B_r = -\frac{\partial}{\partial r} V$$

$$(13) \quad B_\theta = -\frac{1}{r} \frac{\partial}{\partial \theta} V$$

$$(14) \quad B_\phi = -\frac{1}{r \sin \theta} \frac{\partial}{\partial \phi} V$$

By using the VIP 4 Schmidt normalized spherical harmonic coefficients [3], the Jovian magnetic field was calculated in 3D space. The results were then illustrated using the MATLAB GUI shown in Figure 2, in which the user can orient a plane to view a heat map of the magnetic field in that plane. The user can also view the magnetic field as a vector field, and can import an equatorial orbit to visualize its interaction with Jupiter's magnetic field. By validating the implementation of the VIP4 Jovian magnetic field model, we can confidently implement the model in the primary SSDT simulator for Jovian CubeSat costumers.

3.e. Mass Properties Simulator. After developing the Jovian magnetic field GUI, I began working on the spherical air bearing platform. Before working on the platform itself, I had designed a mass properties simulator used to imitate the mass, center of mass, and moment of inertia of a 6U CubeSat. The purpose of this hardware is to simulate the mass properties of a customer's CubeSat so that we can roughly balance the spherical air bearing platform before we receive the spacecraft, which will save time performing the very precise balancing of the actual spacecraft as well as prevent an unstable initial configuration of the platform.

To enable a modular system, the mass properties simulator consists of a perforated aluminum base plate through which small cylindrical mass plugs can be inserted. The mass plugs can be mounted on top of standoffs as well as other plugs in order to vary the mass properties in the z direction, and, when filling the base plate, sum to a total mass above the maximum allowable mass of a 6U CubeSat. A rendering of the mass properties simulator using an example configuration is provided below in Figure 3.

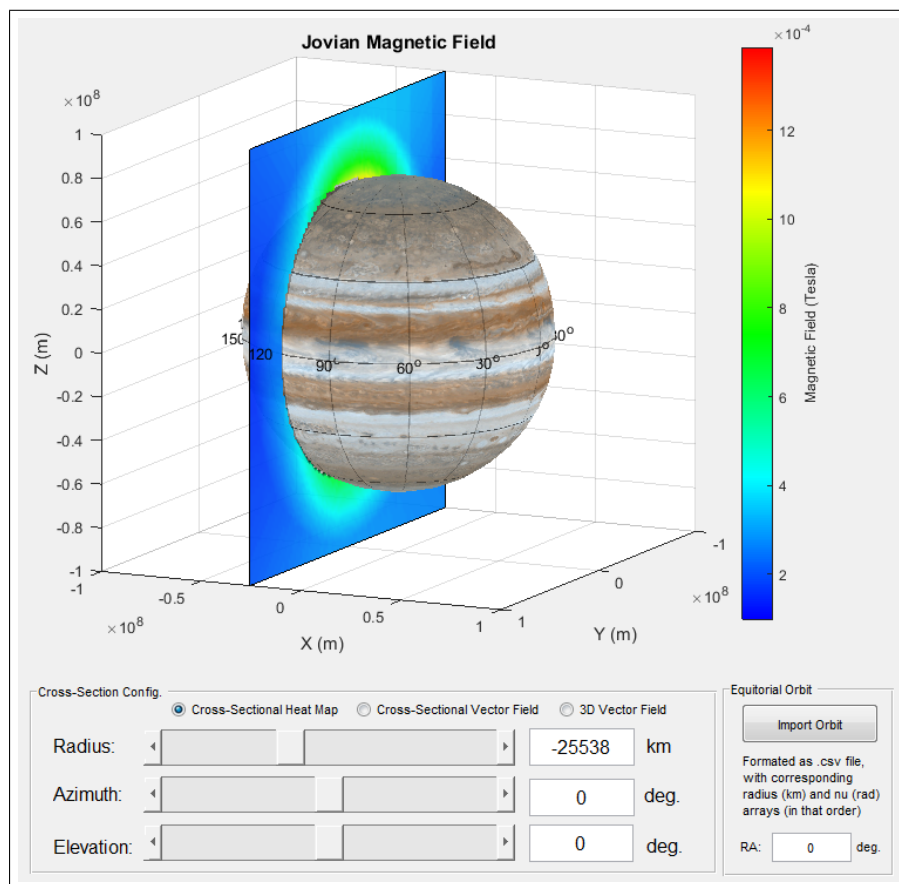


FIGURE 2. Jovian magnetic field GUI used to validate the implementation of magnetic field model.

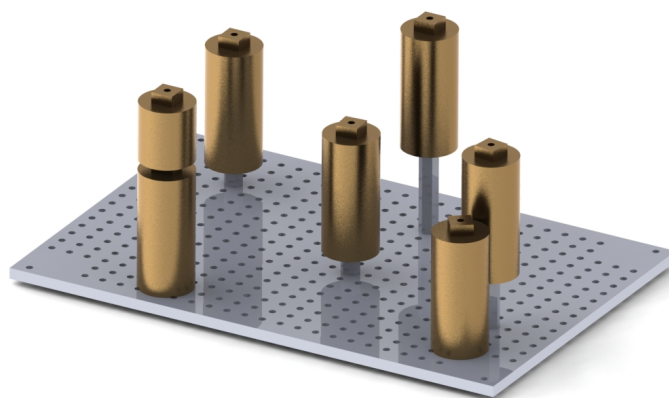


FIGURE 3. Redering of mass properties simulator.

To efficiently adjust the configuration of the Mass Properties Simulator, a MATLAB GUI was developed, as shown in Figure 4. The mass properties calculated in this GUI were verified by evaluation the mass properties of an identical configuration assembled in SolidWorks.

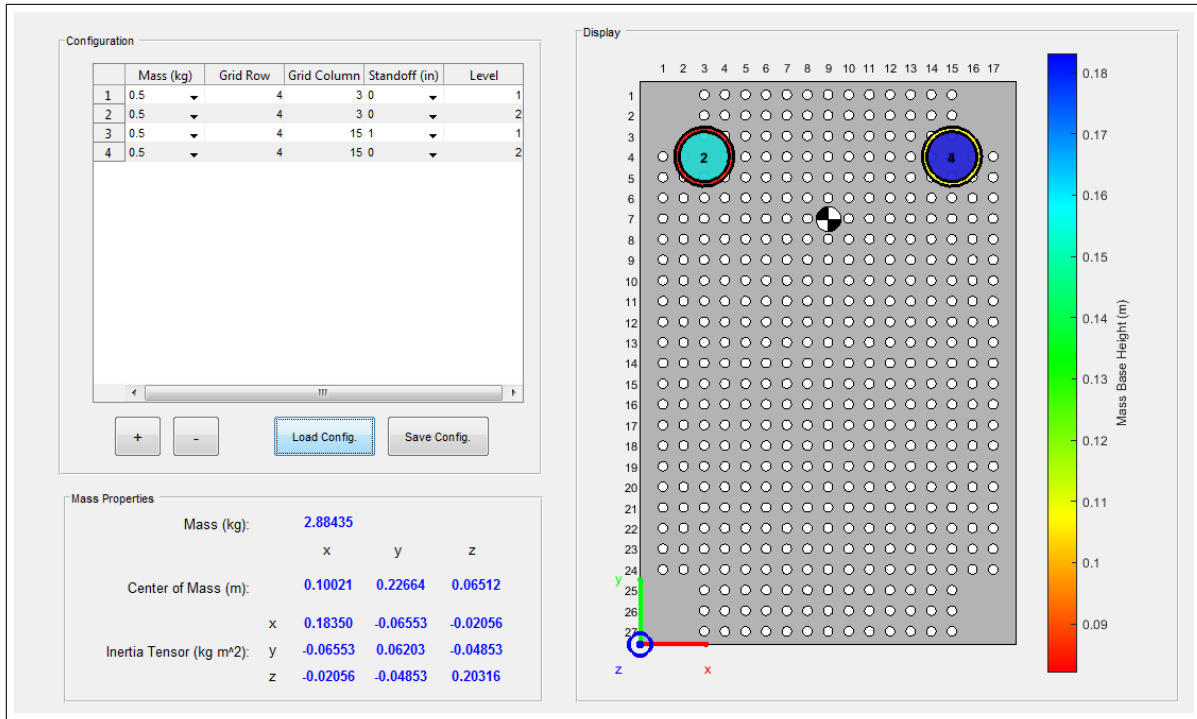


FIGURE 4. Mass properties simulator GUI used to efficiently adjust configuration.

3.f. Spherical Air Bearing Carriage Design. Towards the second half of my internship, I worked towards expanding the capabilities of the previous 1U spherical air bearing carriage by developing a larger carriage to test larger small satellites (e.g., 3U and 6U CubeSats). This carriage was designed to support much of the same components from the SSDT hardware library that will be on the planar carriage, including the BCT Metal XACT and RWp100 reaction wheel, KVH 1760 gyroscope, the Atlas and Emerald electronics boards, and two Thunder Power TP5000 and two PDU boards to support the electronics of the platform and the customer's hardware. The objectives for the carriage were to (a) minimize the values of the moment of inertia tensor to allow observable affects from 6U components with gains similar to those in flight, and (b) minimize the distance between the center of mass and center of rotation to make the carriage well balanced on the spherical air bearing. The constraints of the design were that (a) components must be clear of the "tilt cone" caused by the pedestal of the spherical air bearing and cannot be first to make contact with the pedestal, and (b) the center of mass of the entire system (i.e., carriage + small satellite) must be at or below the center of rotation to prevent instability.

The final layout of the spherical air bearing carriage is shown below in Figure 5. The placement of the system's hardware was chosen to roughly align the system's center of mass with the center of rotation in the X-Y plane, while bringing the components as close as possible to the center of the platform (i.e., placed far enough from the center to prevent collision with the air bearing stand when the platform is tilted at a maximum angle). This layout enabled a very well-balanced carriage according to the mass properties of the components modeled in CAD, with a center of mass to center of rotation offset of only 0.7 mm.

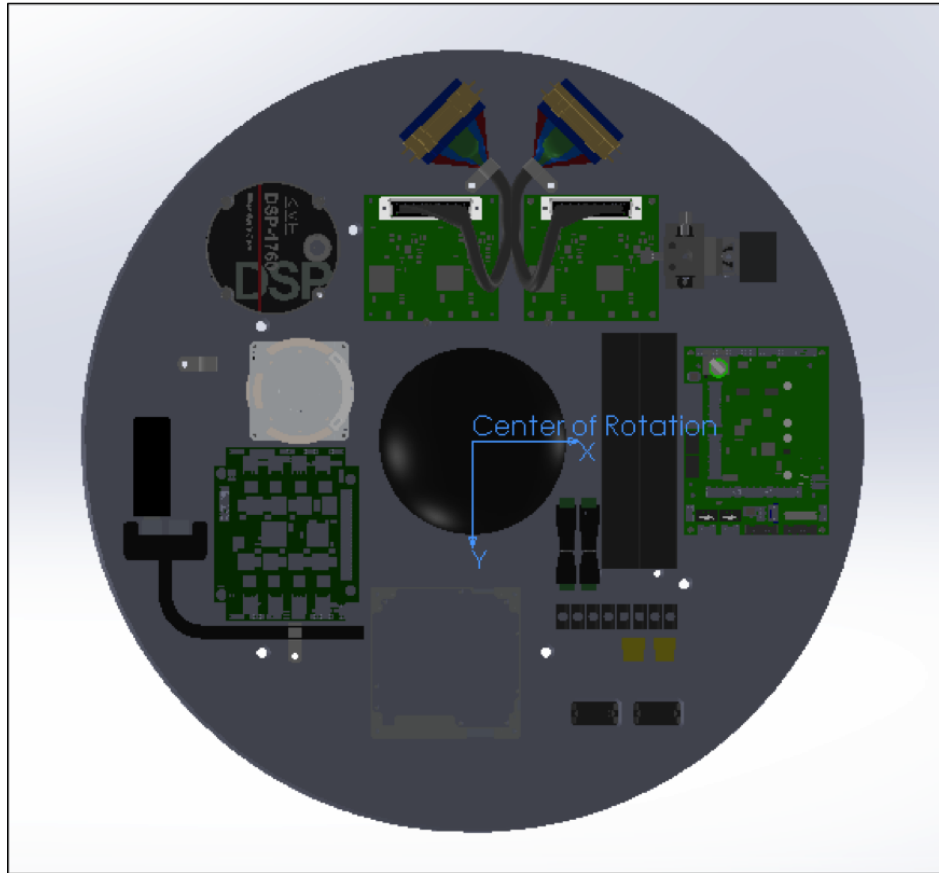


FIGURE 5. Component layout of the final design of the spherical air bearing carriage.

Of course, the mass properties of the components aren't completely accurate; and, some of the smaller parts of the carriage, such as data wires, weren't included in the CAD assembly. Thus, it is not important that the center of mass is perfectly aligned with the center of rotation in the CAD assembly. To allow the center of mass of the system to be shifted to fully balance the carriage, then, a counter-balance assembly was designed. This assembly, as well as the other components of the carriage, are shown in Figure 6. The counter-balance assembly consists of counter-balance blocks, which serve to bring the center of mass below the center of rotation and to coarsely balance the carriage, and the fine-tuning masses, which are used to allow more precise balancing. These

masses can be used to balance the carriage by sliding them along the 80/20 frame of the counter-balance assembly. For even more precise tuning of the center of mass location, the DT12 three-axis linear stage, as shown in Figure 6, can be used.

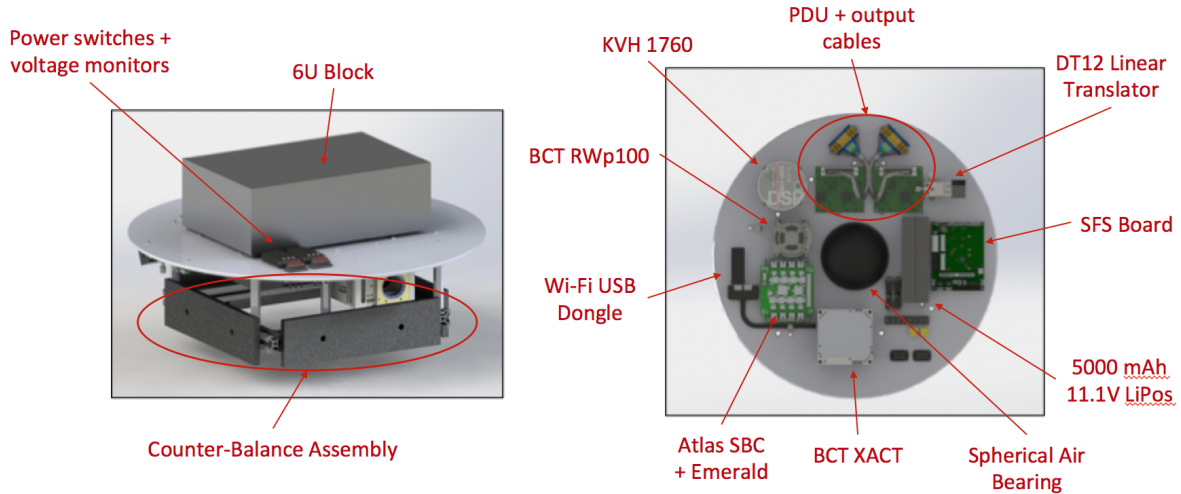


FIGURE 6. Rendering of spherical air bearing carriage, with labeled components

Depending on the mass and center-of-mass location of the small satellite being tested, different combinations of the counter-balance blocks and fine-tuning masses should be used to bring the z-component of the center of mass at or below the center of rotation. To determine appropriate masses of these components, a trade study was conducted regarding the length, width, and height of a counter-balance block, as defined in Figure 7.

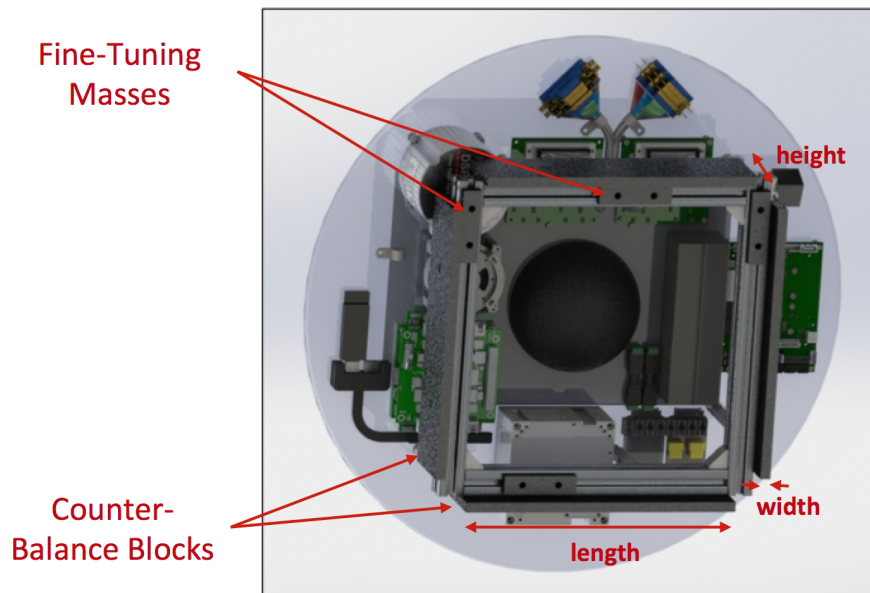


FIGURE 7. Counter-balance assembly

Because the counter-balance assembly was designed to be the first component to contact the pedestal, and should be compressed as much as possible to minimize the moment of inertia, the mounting distance between the bottom of the plate and counter-balance frame and the frame's side length are related according to the maximum tilt angle of the carriage, which, as illustrated in Figure 8, was decided to be 30° (the higher this angle, the further out the frame must be from the pedestal, in turn causing a larger moment of inertia). Further, by setting the vertical component of the center of mass of the carriage to be at the center of rotation, the required mass of the frame can be calculated, in turn constraining the length, width, and height of the counter-balance blocks. Through these two relationships, the width and height of the blocks can be related to the total mass and z-axis moment of inertia of the carriage, as well as the mounting distance described above. The relationships between block width and height and these parameters are illustrated in Figures 9 through 11.

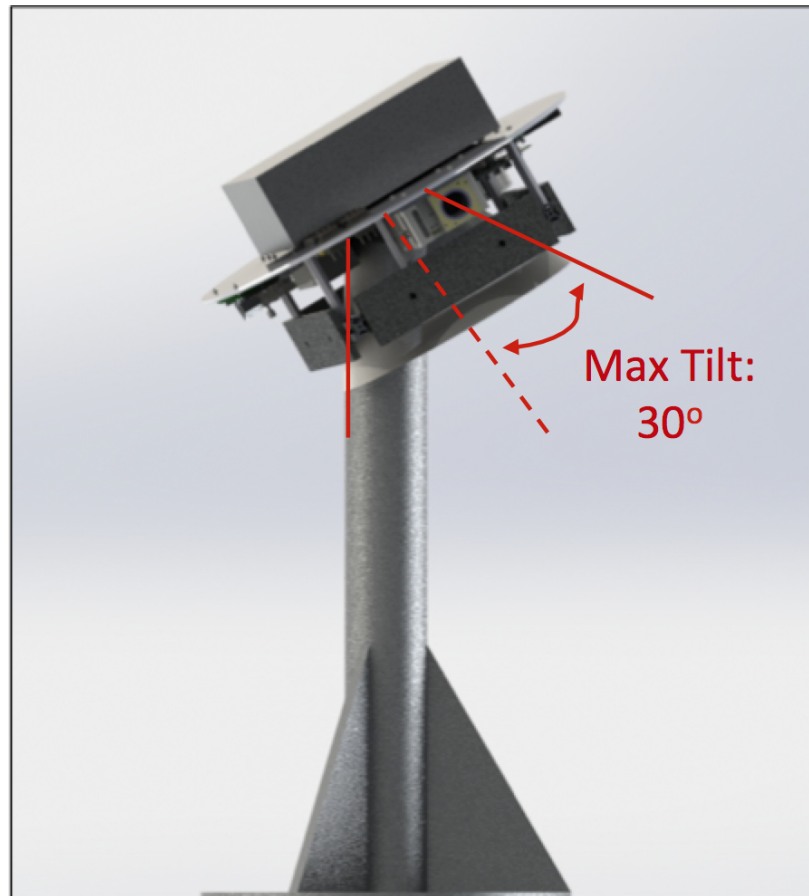


FIGURE 8. Maximum tilt angle determined for spherical air bearing carriage.

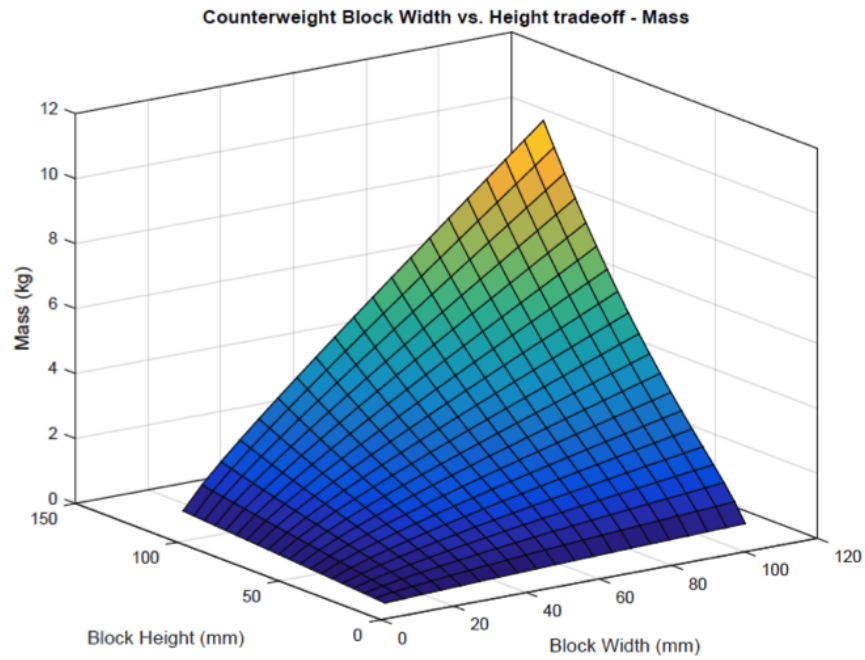


FIGURE 9. Relationship between counter-balance block width, height, and carriage total mass.

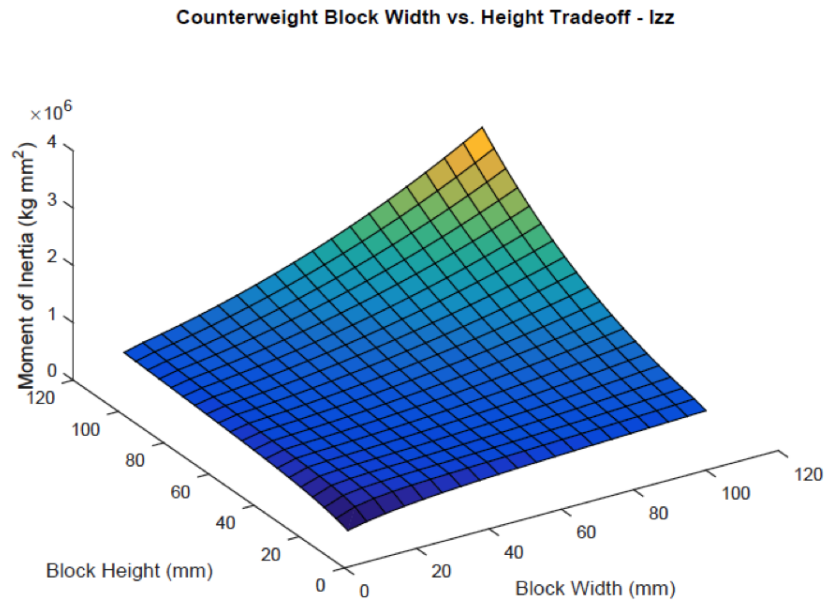


FIGURE 10. Relationship between counter-balance block width, height, and carriage moment of inertia about the vertical axis.

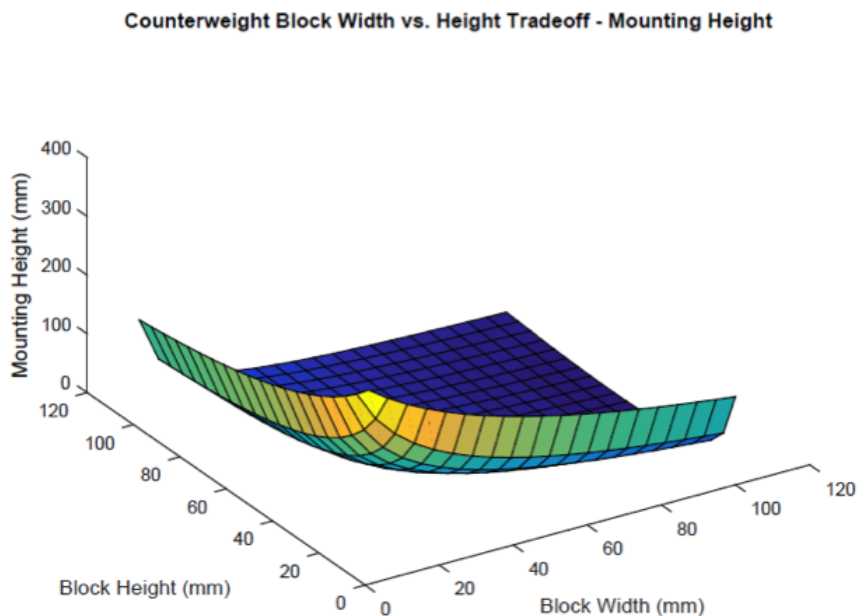


FIGURE 11. Relationship between counter-balance block width, height, and mounting distance between carriage bottom surface and top of counter-balance assembly.

As shown in Figure 10, a larger height and smaller width of the counter-balance block causes a slightly lower carriage moment of inertia about the z-axis (i.e., the vertical axis). This makes sense intuitively, since increasing the block's width, in turn bringing more mass further from the z-axis, directly increases the z-axis moment of inertia. Thus, a low width to height ratio was chosen such that the mounting height was reasonable; exact dimensions were then chosen based on standard sizes of steel blocks and standoffs found on McMaster-Carr.

4. ACKNOWLEDGMENTS

I would like to acknowledge my mentor, Dr. Laura Jones, for her excellent guidance towards the work I did throughout my internship and towards my future in general, her constant willingness to provide me help, and the excitement she instilled in me towards JPL. I would also like to thank the lab members of the SSDT for their help and guidance, including Kevin Lo, William Wilson, Swati Mohan, and fellow intern David Sternberg. Last, I would like to acknowledge the Caltech Student-Faculty Programs for providing me the funding for this incredible experience.

REFERENCES

- [1] Araki, R., Takita, A., Nachaisit, P., Shu, D., and Fujii, Y., *Frictional Characteristics of a Small Aerostatic Linear Bearing*, *Lubricants*, 3, 132-141, 2015.
- [2] Chapman, S., and Bartels, J., *Geomagnetism*, Oxford University Press, New York, 1940.
- [3] Connerney, J. E. P., Acuna, M. H., Ness, N. F., and Satoh, T., *New models of Jupiter's magnetic field constrained by the Io flux tube footprint*, *Journal of Geophysical Research*, 103, A6, 11929-11939, 1998.
- [4] Dourmashkin, Steven J., *Characterization of Effective Friction Between Planar Carriage and FCT Test Plan.*
- [5] Fujii, Y., *Frictional Characteristics of an Aerostatic Linear Bearing*, *Tribology International*, 39, 888-896, 2006.
- [6] Fukui, S., and Yamane, K., *DSMC/MGL Comparisons of Stresses on Slider Air Bearing With Nanometer Spacings*, *IEEE Transactions on Magnetics*, 37, 2153-2155, 2002.
- [7] Wilson, William R., Jones, Laura L., Peck, Mason A., *A Multimodule Planar Air Bearing Testbed for CubeSat-Scale Spacecraft*. Cornell University. July 2013.